

Direct observation of incommensurate magnetism in Hubbard chains

Guillaume Salomon,^{1,*} Joannis Koepsell,¹ Jayadev Vijayan,¹ Timon A. Hilker,¹
Jacopo Nespolo,^{2,3} Lode Pollet,² Immanuel Bloch,^{1,2} and Christian Gross¹

¹*Max-Planck-Institut für Quantenoptik, 85748 Garching, Germany*

²*Fakultät für Physik, Ludwig-Maximilians-Universität, 80799 München, Germany*

³*INO-CNR BEC Center and Dipartimento di Fisica, Università di Trento, 38123 Povo, Italy*

(Dated: March 26, 2018)

The interplay between magnetism and doping is at the origin of exotic strongly correlated electronic phases and can lead to novel forms of magnetic ordering. One example is the emergence of incommensurate spin-density waves with a wave vector that does not match the reciprocal lattice. In one dimension this effect is a hallmark of Luttinger liquid theory, which also describes the low energy physics of the Hubbard model [1]. Here we use a quantum simulator based on ultracold fermions in an optical lattice [2–8] to directly observe such incommensurate spin correlations in doped and spin-imbalanced Hubbard chains using fully spin and density resolved quantum gas microscopy. Doping is found to induce a linear change of the spin-density wave vector in excellent agreement with Luttinger theory predictions. For non-zero polarization we observe a decrease of the wave vector with magnetization as expected from the Heisenberg model in a magnetic field. We trace the microscopic origin of these incommensurate correlations to holes, doublons and excess spins which act as delocalized domain walls for the antiferromagnetic order. Finally, when inducing interchain coupling we observe fundamentally different spin correlations around doublons indicating the formation of a magnetic polaron [9].

One dimensional (1D) quantum systems are paradigmatic examples of the breakdown of Landau-Fermi liquid theory. The free quasiparticle concept present in higher dimensions is replaced by collective excitations leading to striking phenomena such as spin-charge separation [1]. Luttinger liquid theory [10] generically describes the low energy physics of gapless one-dimensional systems ranging from quasi-1D conductors, spin liquids to chiral edge modes in the fractional quantum Hall effect [11]. In particular, the repulsive single-band Hubbard model, which provides a minimal microscopic description of doped antiferromagnets, can be described through this approach. Away from half filling, Luttinger liquid theory predicts incommensurate magnetism with an algebraically decaying incommensurate spin-density wave (SDW) at zero temperature, whose vector varies linearly with density [1]. Also, the presence of a spin imbalance in the 1D Hubbard model can lead to incommensurate spin correlations [12]. Short-range incommensurate magnetism is expected to survive at finite temperature, where conformal field theory arguments predict an exponential decay of the spin correlations with distance [13]. Luttinger liquids were experimentally studied in traditional condensed matter systems such as carbon nanotubes via conductance and scanning tunneling microscopy measurements [14, 15], and in particular, magnetism was studied through neutron scattering on weakly coupled quasi-1D spin-1/2 chains [16, 17] and on ladder systems [18]. In higher dimensions, incommensurate spin-density waves were detected in the underdoped region of certain high- T_c superconductors via neutron scattering [19]. An interpretation in terms of holes organized in stripes was proposed, which results in an effective 1D

description, where the stripes form domain walls in the antiferromagnet. Here we use real space spin and density resolved quantum gas microscopy to directly study the effects of both doping and polarization on finite range spin correlations in the 1D Hubbard model. We measure the linear change in the SDW vector as a function of density in excellent agreement with Quantum Monte-Carlo (QMC) calculations. In presence of a population imbalance, we observe an increase of the SDW wavelength with polarization as predicted by Luttinger liquid theory. We finally report on the evolution of the antiferromagnetic spin correlations around doublons in the crossover from 1D to 2D. We find the magnetic environment around doublons to change fundamentally when spin correlations appear in the transverse direction, suggesting the formation of a magnetic polaron [9].

Our experiments started by loading a balanced two-dimensional degenerate spin mixture of ^6Li atoms in the lowest two Zeeman states $|\uparrow\rangle, |\downarrow\rangle$ into an optical lattice formed by two standing waves with period $d_x = 1.15 \mu\text{m}$ in x direction and $d_y = 2.3 \mu\text{m}$ in y direction (Fig. 1) [5]. The atoms were trapped in a single plane of a vertical lattice with $3.1 \mu\text{m}$ spacing and a depth of $17 E_r^z$ where E_r^i denotes the recoil energy in direction i . The nearest-neighbor tunneling rates were set to $t_x = \hbar \times 410 \text{ Hz}$ at $5 E_r^x$ lattice depth and $t_y = \hbar \times 1.2 \text{ Hz}$ at $27 E_r^y$ to study the one dimensional Hubbard model. By decreasing the lattice depth in the y direction and ramping up the x lattice power to vary t_y/t_x , we can explore the Hubbard model from 1D to 2D. The onsite interaction U was controlled using the broad Feshbach resonance located at 834.1 G and set to $U = 7 t_x$ in the 1D regime. We directly measured the occupation and spin on each

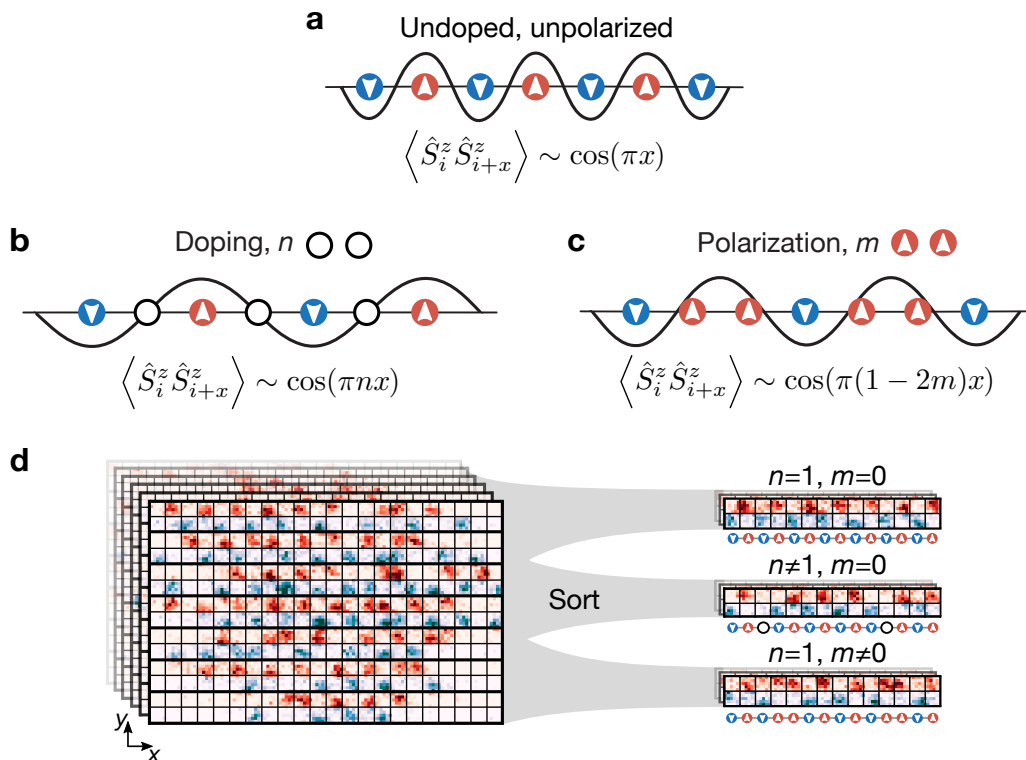


FIG. 1. **Probing incommensurate spin correlations in Hubbard chains.** **a**, Spin correlations in spin-balanced Hubbard chains at half filling ($n = 1$) form at a commensurate wave vector π . **b**, When the system is doped ($n \neq 1$), incommensurate spin correlations at a wave vector πn develop due to delocalized holes and doublons, which act as quantum domain walls stretching the distance between antiferromagnetically correlated spins. **c**, At finite polarization $m \neq 0$, incommensurate spin correlations at a wave vector $\pi(1 - 2m)$ arise due to excess spins. **d**, Left: Single-spin and density-resolved experimental images, each containing 7 independent Hubbard chains along y separated by thick lines where spins \uparrow (\downarrow) are represented in red (blue). Right: In post-analysis we group the data by magnetization and doping to analyze their individual effect on spin correlations along x .

lattice site by first freezing the atomic motion before a local Stern-Gerlach like splitting of the spin components in a superlattice along y [5] (Fig. 1). Finally we detected the atoms via Raman sideband cooling [20]. Thanks to the ultimate resolution of our detection down to single atoms and spins, we are able to group our data according to total spin $S^z = (N_\uparrow - N_\downarrow)/2$ and total atom number $N = N_\uparrow + N_\downarrow$, that is, the sum of the up and down spin number in each chain. These conserved quantities fluctuate for different chains and experimental runs (see Supplementary Information), however, data grouping allows us to individually explore the effect of doping and spin imbalance (Fig. 1).

We first study the evolution of antiferromagnetic spin correlations along 1D chains as a function of doping. The correlations are quantified by the two-point correlation function $C(x) = 4\langle S_i^z S_{i+x}^z \rangle_{\bullet_i \bullet_{i+x}}$ conditioned on the sites $i, i+x$ being singly occupied (filled circles). Experimentally, we prepared Hubbard chains with up to $N = 23$ atoms and post-selected the experimental outcomes to the $S^z = 0$ sector to first consider the effects of doping only. Due to the underlying harmonic confinement, the

atomic cloud is inhomogeneous and in the spirit of a local density approximation we define the density n as the mean occupation calculated over the sites connecting i to $i+x$ for each value of N (see Supplementary Information). From Luttinger liquid theory one expects the wave vector of the SDW to be $k_{\text{SDW}} = 2k_F = \pi n$ defining the Fermi wave vector k_F . At finite temperature and large distances $x \gtrsim k_F^{-1}$, the spin correlations are predicted to decay exponentially [1]:

$$C(x) \simeq A e^{-\frac{x}{\xi}} \cos(\pi n x), \quad (1)$$

where A is a non-universal constant and ξ is the temperature-dependent correlation length that weakly varies [1] with density at $U/t = 7$. We determined A and ξ from an exponential fit of $C(x)$ at half filling ($n = 1$) for $x = 2, \dots, 6$ yielding $A = 0.49(4)$, $\xi = 1.6(1)$ (Fig. 2a) where all distances are expressed in units of the lattice constant d_x . Away from half filling, we observe a linear increase of the SDW vector both for hole and charge doping as revealed by a Fourier transform of the rescaled spin correlation $C(k) = \mathcal{F}\{A^{-1}e^{x/\xi}C(x)\}$. For a quantitative comparison with theory, we show in Fig. 2c the spin cor-

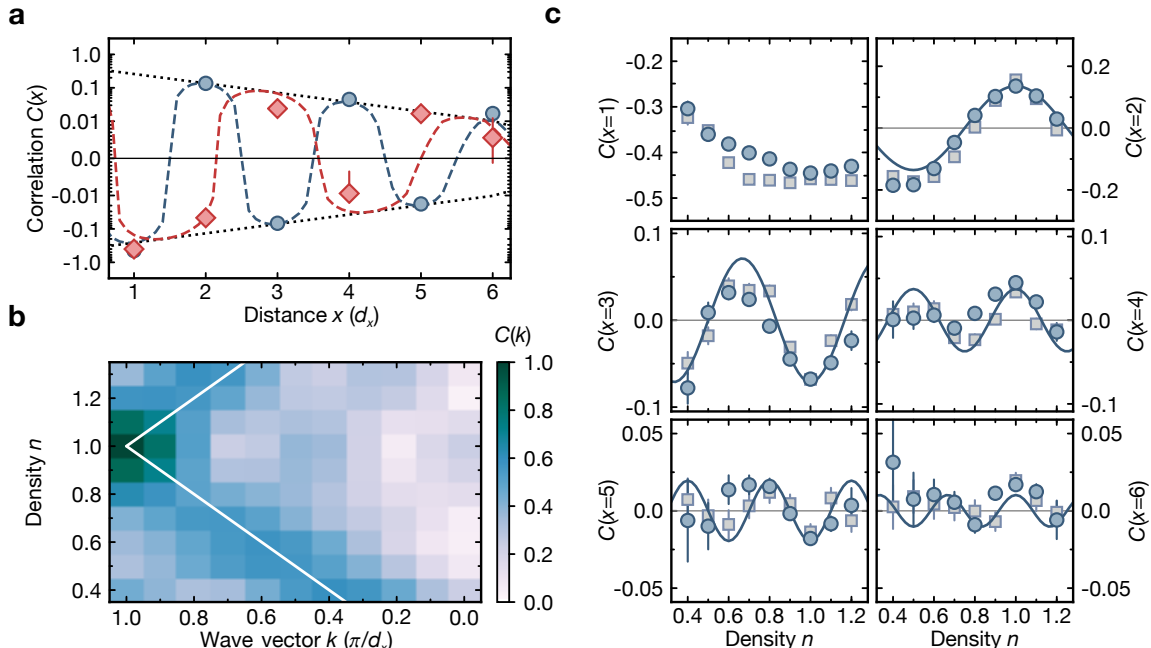


FIG. 2. **Incommensurate spin correlations vs doping.** **a**, Spin correlations $C(x)$ at half filling (blue) and at $n = 0.7$ (red). The dotted lines show the decay obtained from an exponential fit of the rectified spin correlations $(-1)^x C(x)$ at half filling. The dashed lines are the Luttinger liquid predictions using the amplitude and decay length obtained from a fit of the $n = 1$ experimental data. The sign change observed for $d \geq 2$ in the doped case originates from delocalized holes acting as quantum domain walls, which stretch the distance between antiferromagnetically correlated spins. **b**, Away from half filling the normalized Fourier transform of the spin correlations $C(k)$ reveals a linear increase of the SDW wave vector with density. The white line is the Luttinger liquid result $k_{\text{SDW}} = \pi n$. **c**, Spin correlations $C(x)$ vs density at fixed distances $x = 1, \dots, 6$ (blue dots) compared to QMC calculations at $T = 0.29 t_x$ (gray squares). The measured densities are binned in intervals of 0.1. The blue lines are the Luttinger liquid prediction with wave vectors πn using the amplitude and decay length extracted from the fit in **a**. Around unity filling oscillations up to distances of $x = 6$ are visible as a function of density in agreement with Luttinger liquid theory. Errorbars denote standard error of the mean.

relations $C(x)$ as a function of density n together with QMC calculations for a homogeneous system at temperature $T = 0.29 t_x$ and the long distance Luttinger prediction of Eq. 1. The spin correlations oscillate with a periodicity $k_{\text{SDW}} = \pi n$ as expected from Luttinger theory. We attribute the microscopic origin of the incommensurate correlations to delocalized doublons and holes, increasing the distance between antiferromagnetically correlated spins [21, 22] and thus, the wavelength of the SDW.

Incommensurate spin correlations are also expected to appear in the one-dimensional Hubbard model when a spin-imbalance is introduced. To isolate the effect of polarization from the influence of doping, we consider the two-point spin correlations $C(\tilde{x}) = 4\langle S_i^z S_{i+\tilde{x}}^z \rangle$ in squeezed space obtained by removing holes and doublons from the chain in post-analysis [22]. In squeezed space [23, 24] and for large U/t_x , the system is described by a spin-1/2 antiferromagnetic Heisenberg model at a polarization $m = S^z/N_s$, where N_s is the number of

singly occupied sites (see Supplementary Information). For the Heisenberg chain, Luttinger liquid theory predicts at large distances incommensurate spin correlations linear in the polarization [1] m :

$$C(\tilde{x}) \simeq A_m e^{-\frac{\tilde{x}}{\xi_m}} \cos(\pi(1 - 2m)\tilde{x}) \quad (2)$$

where A_m, ξ_m are the magnetization and temperature-dependent amplitude and correlation length. The SDW wavelength measured by $C(\tilde{x})$ is thus expected to increase away from $m = 0$. In Fig. 3a we show $C(\tilde{x})$ for two polarizations of the chain $m = -0.12$ and 0. We observe first a strong decrease of the amplitude of the spin correlations at fixed distance for finite m compared to $m = 0$. This behavior is expected from conformal field theory which predicts the exponential decay to be stronger due to a larger zero-temperature critical exponent [25]. To reveal the wave vector of the SDW we computed the Fourier transform of the spin correlations in squeezed space $C(\tilde{k}) = \mathcal{F}\{C(\tilde{x})\}$ which qualitatively shows a linear decrease of the wave vector with m

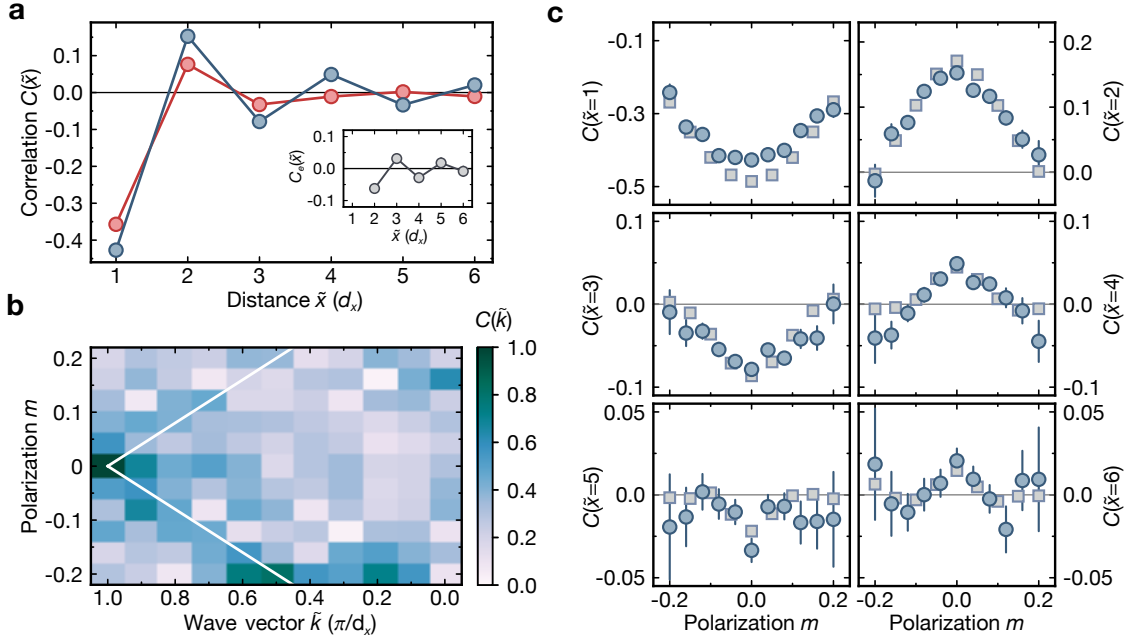


FIG. 3. **Incommensurate spin correlations vs polarization.** **a**, Spin correlations in squeezed space $C(\tilde{x})$ at $m = 0$ (blue) and $m = -0.12$ (red). A sign change is visible at distance $d > 4$ reflecting an increase of the SDW wavelength away from $m = 0$. Inset: In a spin-imbalanced gas at $m = -0.12$ the distance between antiferromagnetically correlated spins is stretched as revealed by the sign changes in the spin correlations C_e across majority spins (black). **b**, Normalized Fourier transform $C(\tilde{k})$ of $C(\tilde{x})$ qualitatively revealing a linear change of the SDW vector in agreement with the Luttinger liquid prediction $\pi(1 - 2m)$ (white line). **c**, Experimental spin correlations $C(\tilde{x})$ vs magnetization m at fixed distances $\tilde{x} = 1, \dots, 6$ (blue dots) compared to QMC calculations at $T/t_x = 0.25$ and half filling (gray squares). Binning of the magnetization is in intervals of 0.04 and errorbars denote one standard error of the mean.

(Fig. 3b). We also compare the squeezed space spin correlations at fixed distance to QMC calculations at half filling for $T/t_x = 0.25$ of the Hubbard chain (Fig. 3c). The good agreement between experiment and theory validates the use of the squeezed space concept away from $m = 0$. We attribute the remaining small discrepancy at short distances to our finite detection efficiency (97%), which leads to wrongly detected holes resulting in an error in the construction of squeezed space. We also expect a small bias towards lower correlations due to the analysis in squeezed space, where contributions from lower density areas show smaller correlations [21]. Similar to the doped case [21], we now study the microscopic origin of these incommensurate spin correlations. We analyze the spin environment around the majority spins $C_e(\tilde{x}) = 4\langle S_i^z S_{i+\tilde{x}}^z \rangle_{S^z \sigma_{i+1} > 0}$ by measuring the conditional expectation value of the spin correlations in squeezed space for distances $\tilde{x} \geq 2$. The correlations are conditioned on the spin σ on site $i + 1$ being parallel to the chain magnetization S^z (Fig. 3a). We observe that the sign of the oscillating part in the spin correlations across majority spins changes compared to the unpolar-

ized case revealing that excess spins act as delocalized domain walls for the antiferromagnetic order (Fig. 3a). Thus, their main effect is to increase the distance between antiferromagnetically correlated spins resulting in an increase of the SDW wavelength as measured by $C(\tilde{x})$. To formally connect this phenomenon to the effect of doping one can consider the excess spins $N_\uparrow - N_\downarrow = N_e$ and write the polarization as $m = n_e/2$, where n_e is the excess spin density. This leads to a variation of the SDW with distance proportional to $\cos(\pi\bar{n}_e x)$, where $\bar{n}_e = 1 - n_e$, in direct analogy to Eq. 1 underlining the similarity between the effects of doping and polarization. Polarized synthetic Hubbard models have recently also been studied in two dimensions and the emergence of anisotropic spin correlations has been observed [8].

We now explore the evolution of the spin correlations in the 1D-2D crossover, a situation relevant to quasi-1D antiferromagnets [17]. Whereas in 1D there is no magnetic energy cost associated with the delocalization of holes and doublons, this phenomenon is expected to breakdown in higher dimensions. In a 2D antiferromagnetic background the motion of holes and doublons leads to strings of flipped spins resulting in the confinement of spin and

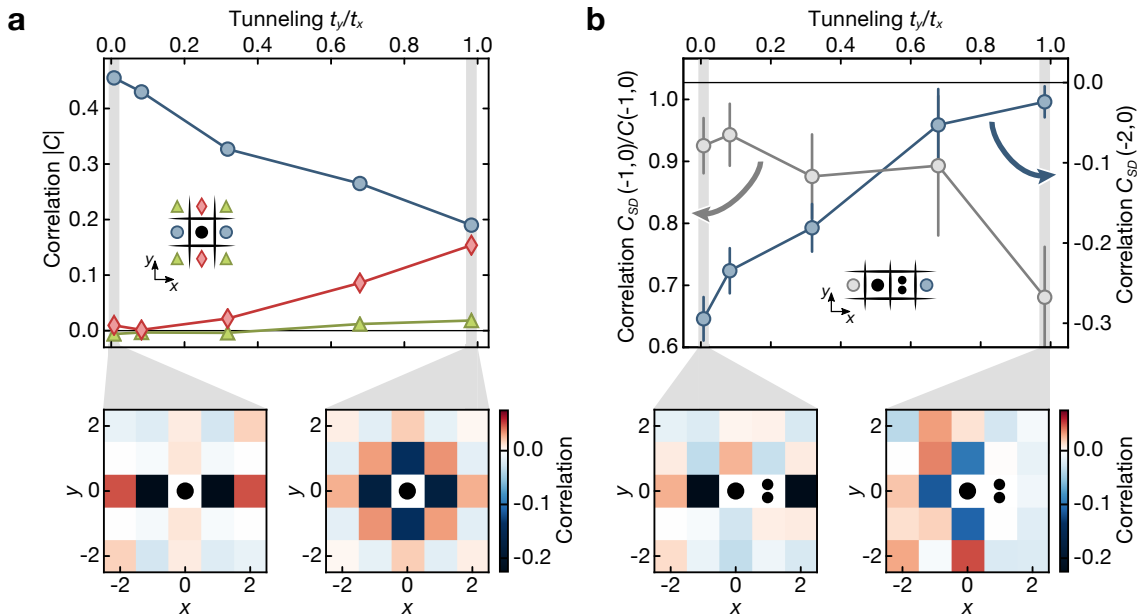


FIG. 4. **Spin correlations in the 1D-2D crossover.** **a**, Spin correlations $C(x, y)$ as a function of the ratio t_y/t_x : $|C(1, 0)|$ (blue circles), $|C(0, 1)|$ (red diamonds) and $C(1, 1)$ (green triangles) at $U/t_x=14$. The spin correlations along x decrease as spin correlations develop in y -direction. The pictures below show the 2D spin correlations amplitudes $C(x, y)$ in the 1D (left) and 2D (right) limits. **b**, Spin correlations across doublons $C_{SD}(2, 0)$ (blue) and next to it $C_{SD}(-1, 0)/C(-1, 0)$ (gray) along the x direction. Antiferromagnetic correlations across doublons, at the origin of incommensurate correlations in the 1D limit, are strongly suppressed as spin correlations develop in 2D. In this limit the delocalization of doublons also leads to a reduction of antiferromagnetic correlations on neighbouring sites, indicating the formation of a magnetic polaron. Figures below show the spin correlations $C_{SD}(x, y)$ between sites $(0, 0)$ and (x, y) conditioned on finding a doublon on site $(1, 0)$ in the 1D (left) and 2D (right) case.

charge [9, 26]. The spin correlations around doublons and holes are thus expected to show qualitative differences in the crossover from 1D to 2D [9]. We prepared 2D clouds with up to 70 atoms and studied spin correlations while varying t_y/t_x between 0 and 1 keeping $U/t_x = 14$ constant (see Supplementary Information). When increasing t_y/t_x , we first observe a decrease in the amplitude of the spin correlations $C(x, y) = 4\langle S_{i,j}^z S_{i+x,j+y}^z \rangle_{\bullet_{i,j} \bullet_{i+x,j+y}}$ along x and the emergence of spin correlations in the transverse directions (Fig. 4a) [27]. This decrease is expected even at zero temperature and half filling, where the nearest-neighbor spin correlations $C(1)$ change from -0.6 to -0.36 due to the higher coordination number modifying the quantum fluctuations [4].

Next we study the magnetic environment around doublons in the dimensional crossover from 1D to 2D through $C_{SD}(x, y) = 4\langle S_{i,j}^z S_{i+x,j+y}^z \rangle_{\bullet_{i,j} \circ_{i+1,j} \bullet_{i+x,j+y}}$ where the empty circle denotes a doublon located at site $(i+1, j)$ (see Supplementary Information). We find that the spin correlations across doublons, $C_{SD}(2, 0)$, are strongly suppressed while 2D spin correlations develop, which is in stark contrast to the 1D case (Fig. 4b). Due

to the harmonic confinement the few double occupancies are located in the center of the trap, where the average density is highest and where magnetic correlations are expected to compete with doublon delocalization. In addition to the vanishingly small antiferromagnetic correlations across doublons, we observe a reduction of the nearest-neighbor spin correlations in its vicinity $C_{SD}(-1, 0)/C(-1, 0)$ to about 70% compared to the undoped case (Fig. 4b). This indicates the formation of a magnetic polaron [9], which in the extreme limit $U/t \rightarrow \infty$ corresponds to the Nagaoka polaron [28].

Through the direct simultaneous measurement of both density and spin in the doped and spin-imbalanced 1D Hubbard model, we shed light onto the connection between incommensurate spin correlations and the microscopic degrees of freedom. The spin environment around doublons was found to differ drastically in the 1D and 2D cases calling for further experimental studies of the formation of magnetic polarons in homogeneous systems [9, 29]. Another interesting extension of this work is the study of spin correlations as a function of the number of coupled chains where the parity of the latter is pre-

dicted to lead to striking differences between even and odd cases similar to the problem of half-integer and integer spin chains [30, 31]. At low enough temperature the study of spin and density correlations in hole-doped coupled chains is also expected to reveal a binding of holes to form stripes which directly extends the domain-wall concept discussed here to 2D [32]. A study of such effects through quantum gas microscopy can offer new microscopic insights into the physics of the doped repulsive Hubbard model.

SUPPLEMENTARY INFORMATION:

ULTRACOLD LATTICE GAS PREPARATION

The experimental protocol used in the experiments reported here closely followed our previous work [21]. Our experiments started with a degenerate spin mixture of ${}^6\text{Li}$ atoms in the lowest two Zeeman states $|\pm\rangle = |F = 1/2, m_F = \pm 1/2\rangle$ trapped in a single plane of a vertical optical lattice. The lattice spacing was $3.1\ \mu\text{m}$ and the depth $17 E_r^z$ (resp. $27 E_r^z$) in the 1D (crossover) case, where $E_r^i = \hbar^2/8md_i^2$ is the recoil energy, m the atomic mass and d_i the lattice spacing along direction i . The total atom number N of the cloud was tuned by varying the depth of a radial trap at the endpoint of the evaporative cooling procedure [20]. To simulate the single-band one-dimensional (1D) Hubbard model, we first prepared 1D systems by ramping up the large spacing component ($d_y = 2.3\ \mu\text{m}$) of an optical superlattice in y -direction. The lattice was ramped linearly in two steps, first, to $15 E_r^y$ in 55 ms and then to $27 E_r^y$ in 45 ms, which results in a final transverse tunneling of $t_y = \hbar \times 1.3\ \text{Hz}$. With a delay of 10 ms with respect to the start of the y -lattice ramp, the lattice along the tubes (x -direction, spacing $d_x = 1.15\ \mu\text{m}$) was turned on. The chosen ramp was again composed of two linear parts, the first was a ramp to $3 E_r^x$ in 45 ms, the second to $5 E_r^x$ in 55 ms. The scattering length was simultaneously increased from $530 a_B$ to $2000 a_B$ using a magnetic offset field close to the Feshbach resonance located at 834 G. At the end of the ramps the tunneling along the Hubbard chains reached $t_x = \hbar \times 400\ \text{Hz}$ and the onsite interaction $U = \hbar \times 2.9\ \text{kHz}$. The latter is calculated from the ground band Wannier functions neglecting higher band corrections [33]. The corresponding final superexchange coupling was $J_x = 4t_x^2/U = \hbar \times 220\ \text{Hz}$.

To explore the Hubbard model in the crossover from 1D to 2D we first ramped up the large spacing component of the superlattice in y -direction to $0.2 E_r^y$ in 60 ms and then to depths varying between $5 E_r^y$ and $27 E_r^y$ in 220 ms. The x -lattice ramp to depths varying between $9 E_r^x$ and $10.6 E_r^x$ in 280 ms started simultaneously with the second part of the y -lattice ramp. The magnetic offset field was adjusted to maintain a constant ratio $U/t_x = 14$ at the

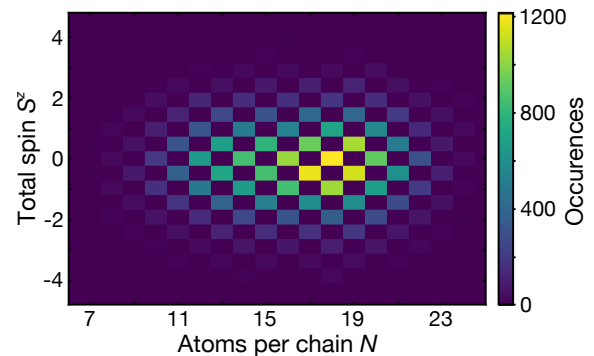


FIG. S1. **Chain statistics.** Hubbard chain statistics for a typical dataset containing 5240 shots. The total spin S^z and total atom number N of individual Hubbard chains are conserved quantities of the Hamiltonian for each experimental run. However, they fluctuate for different experimental realizations allowing to explore individually the effects of doping and polarization through data grouping.

end of the ramps. A local Stern-Gerlach detection technique [5] operating at a transverse magnetic field gradient of 95 G/cm was used to detect both the spin and the density on each lattice site with a fidelity of 97%.

DATA ANALYSIS

Thanks to our local access to both spin and occupation on each lattice site in a single experimental run, we can group each Hubbard chain data by $\{j, N, S^z\}$, where j is the coordinate of the Hubbard chain in y -direction, N and S^z are total atom number and spin. This allows us to explore different filling and spin sectors (Fig. S1). To study the effect of doping on spin correlations we only analyzed the data in the $S^z = 0$ sector. The density profile along x is inhomogeneous and dependent on N and j , which is caused by the underlying harmonic confinement of $\omega = 2\pi \times 200(20)\text{Hz}$. For each pair $\{j, N\}$ we computed a mean density profile $n_j(i, N)$ by averaging the occupation on each site i over different experimental realizations (Fig. S2). The reported density at which spin correlations between sites i and $i+x$ have been analyzed is the mean density between the two points $n_j(i, x, N) = \frac{1}{x} \sum_{k=i}^{i+x} n_j(k, N)$.

To highlight the oscillatory behavior of the spin correlations as a function of density we considered the two-point spin correlations between sites i and $i+x$, conditioned on having single occupancies on these sites for each pair $\{j, N\}$:

$$C_{i,j,N}(x) = 4 \langle S_i^z S_{i+x}^z \rangle_{\bullet_i, \bullet_{i+x}, j, N} + c(N) \quad (3)$$

where the filled circles denote single occupancy, the brackets an average over experimental runs and $c(N)$ is a finite size offset that depends on the atom number N and temperature, which we experimentally found to

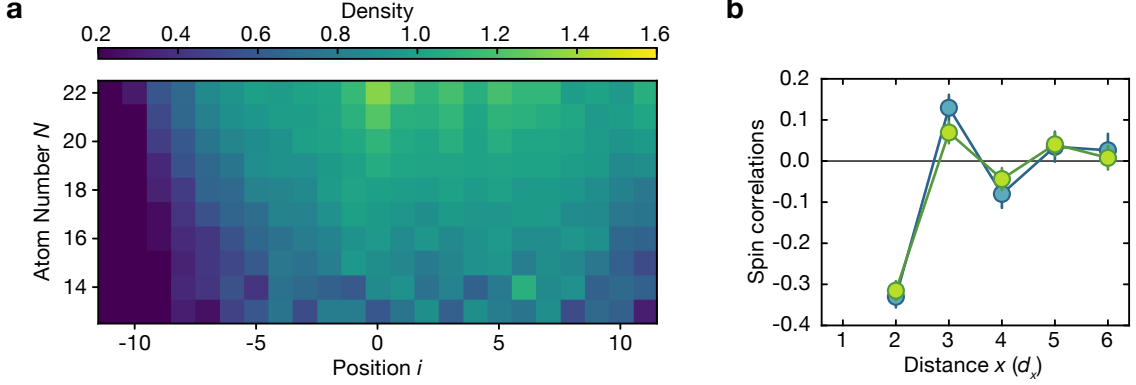


FIG. S2. **Density properties of the 1D clouds.** **a**, Density profiles $n_0(i, N)$ of the chain located at the center in y -direction ($j = 0$). **b**, Antiferromagnetic spin correlations across a hole fixed at $d_x = 1$ (green) or a doublon (blue) measured by $C^{dw}(x)$. The correlation signal is shifted by the hole which is the microscopic origin of the incommensurate spin correlations away from half filling in the spin-balanced case.

be well described by $c(N) = \frac{1}{N-1} - 0.04(5)$ [21]. We also analyzed the data in terms of the corresponding connected correlator and found them to agree with the non-connected version above within statistical uncertainty. This check was performed also for all other non-connected correlators we use in this manuscript. Due to the absence of density-density correlations beyond $d_x = 1$, this correlation function can be understood as being a renormalized 2-points spin correlation $C_{i,j,N}(x) \simeq \frac{4\langle S_i^z S_{i+x}^z \rangle_{j,N-c(N)}}{n_j(i,x,N)^2}$ [21]. We finally grouped all the $C_{i,j,N}(x)$ by their density $n_j(i,x,N)$ in bins of width $\Delta n = 0.1$ to compute the average spin correlation $C(x)$ for each n shown in Fig. 2 of the main text.

The microscopic origin of the incommensurate SDW is revealed by the spin correlations across holes and double occupancies shown in Fig. S2b:

$$C_{i,y,N}^{dw}(x) = 4\langle S_i^z S_{i+x}^z \rangle_{\bullet_{i,\circ_{i+1}}\bullet_{i+x},y,N} + c(N), \quad (4)$$

where filled circles denote the condition of having single occupancies on sites $i, i+x$ and the empty circles denote a doublon or a hole on site $i+1$. The brackets indicate averaging over all experimental realizations, in which these conditions are fulfilled. Both the holes and the doublons displace the spin correlations leading to an increase of their wavelength.

To separate the effect of polarization on the spin correlations from the charge sector, we studied spin correlations in squeezed space. Here, we extend the squeezed space concept to finite U by removing doublons and holes only when these are not nearest-neighbors. The latter condition is supported by the strong doublon-hole bunching at $d = 1$ measured by $g_2(x) = -1 + \langle d_0 h_x \rangle / \langle d_0 \rangle \langle h_x \rangle$

(see Fig. S3a), which we attribute to quantum fluctuations. The full dataset in this measurement consisted of 6474 experimental runs, in which we prepared the chains close to half filling in the center. This lead to chains with up to $N = 15$ atoms. We decided to use the squeezed space analysis instead of post-selecting the data to the zero hole and doublon sector to improve our statistics. Within statistical uncertainties, the post-selected data is consistent with these squeezed state results.

The spin correlations in squeezed space, indicated by \tilde{i} and \tilde{x} , are defined as:

$$C_{i,j,N_s,S^z}^c(\tilde{x}) = 4\langle S_i^z S_{i+\tilde{x}}^z \rangle + c_{sq}(N_s, S^z), \quad (5)$$

where N_s is the number of singly occupied sites including nearest neighbor doublon-hole pairs. We again take into account a finite size offset $c_{sq}(N_s, S^z) = \frac{1}{N_s-1} - \frac{4(S^z)^2}{N_s(N_s-1)} - 0.05(5)$ in analogy to $c(N)$ [21]. The magnetization of the effective Heisenberg chain in squeezed space is defined as $m = S^z/N_s$. We grouped all the $C_{i,j,N_s,S^z}^c(\tilde{x})$ by their polarization m in bins of width $\Delta m = 0.04$ to compute the average spin correlation C shown in Fig. 3 of the main text. The Fourier transform shown in Fig. 3b of the main text has been calculated without the nearest-neighbor correlations (i.e. for $\tilde{x} \geq 2$) to avoid short distance effects.

Similar to the hole and doublon case, the microscopic origin of the polarization dependence of the SDW wavelength can be revealed by the oscillating part in the spin correlations across majority spins:

$$C_{i,j,S^z,N_s}^e(\tilde{x}) = 4\langle S_i^z S_{i+\tilde{x}}^z \rangle_{S^z \sigma_{i+1} > 0} - c_{sq,2}(N_s, S^z), \quad (6)$$

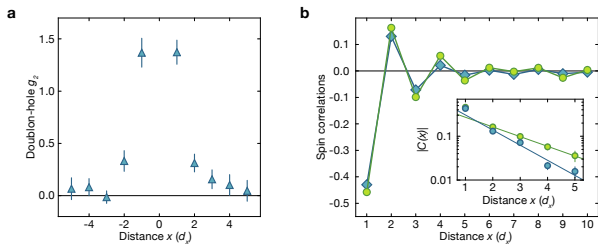


FIG. S3. **Spin correlations in squeezed space.** **a**, Doublon-Hole correlations measured by $g_2(x)$. The strong bunching at $|x| = 1$ reveals neighboring doublon-hole pairs as mostly stemming from quantum fluctuations. This justifies our extension of the squeezed space concept away from $U \rightarrow \infty$. **b**, Spin correlations in the zero magnetization sector in the center of the cloud. The averaging over different polarization (blue) results in a faster decay of the spin correlations with distance x in squeezed space compared to the $S^z = 0$ sector (green). Exponential fits of the correlation envelope for distances $x = 2, \dots, 6$ yield $\xi_{avg} = 1.3(1)$ without magnetization post-selection and $\xi_0 = 2(1)$ in the $S^z = 0$ sector.

where the spin σ on site $\tilde{i} + 1$ is parallel to the total magnetization in the chain S^z and $c_{sq,2}(N_s, S^z) = \frac{2}{(N_s - 1)(N_s - 2)} (2(S^z)^2 - 2|S^z| - N_s/2 + 1)$ is the corresponding finite size and finite magnetization offset for uncorrelated spins. The brackets indicate the average over all experimental realization where this condition is fulfilled. We finally averaged the correlator over $\{i, j, S^z, N_s\}$ and binned $m = 0.12 \pm 0.02$ to obtain $C_e(\tilde{x})$ presented on Fig. 3 of the main text. The sign change of the spin correlations at $\tilde{x} \geq 2$ reveal that the excess magnetization is carried by delocalized spinons. These stretch spin correlations and lead to incommensurate magnetism when $m \neq 0$.

In the dimensional crossover and 2D regime we prepared anisotropic samples consisting of about five coupled Hubbard chains (Fig. S4). Similarly to the 1D case, the spin correlations were calculated on singly occupied sites through $C_{\vec{n}}(\vec{r}) = 4 \langle S_{\vec{n}}^z S_{\vec{n}+\vec{r}}^z \rangle_{\bullet_{\vec{n}}, \bullet_{\vec{n}+\vec{r}}}$ averaged over all sites \vec{n} . When studying spin correlations around double occupancies and holes in the crossover, we took care to minimize biasing of the correlator by a possibly distorted magnetic background around quantum fluctuation induced doublon-hole pairs. The strong bunching observed in $g_2(\vec{r})$ (see Fig. S4) on nearest neighbor scale identifies a strong contribution of quantum fluctuations to these. Hence, we discarded from the analysis of the spin correlations any doublons having one of its nearest neighbor unoccupied.

QUANTUM MONTE-CARLO CALCULATIONS

The Quantum Monte Carlo (QMC) results shown in the present work are obtained in a similar fashion as those found in [5]. Simulating the fermionic system without sign problem is made possible by the mapping between the one-dimensional fermionic Hubbard model and a system of two hard-core bosonic species with on-site interspecies interactions [34].

We make use of the worm algorithm [35] in the implementation of Ref. [36]. This algorithm exhibits a linear scaling in the system volume when simulating the resulting bosonic model. The spin S_i at site i of the fermionic model maps onto a diagonal observable with respect to the Fock basis $\{|\dots, n_j, \dots\rangle\}$ of the bosonic model, proportional to the differences in the occupation numbers of the bosonic particles at the same site.

The simulations were all carried out in the grand-canonical ensemble. The system consisted of a homogeneous lattice of $L = 20$ sites with hard-wall boundary conditions. This size was checked to be already large enough to avoid finite size corrections. Note however that the correlations are affected by an unavoidable systematic offset which scales as $1/N$ and which was corrected for in the analysis as explained above.

To better mimic the measurement procedure of the actual experiment, we saved the raw QMC configurations and performed the analysis off-line. In this process, care must be taken to make sure that subsequent configurations are decorrelated. A further blocking and jackknife estimation was used to rule out any residual correlation.

The off-line analyses were subject to the same filtering procedures for the occupation and magnetization sector as it was done in the experimental procedure. In order to gather enough statistics for the different values of the density accessible in the experiment, we tuned the chemical potentials of the two bosonic species so as to have symmetric mixtures with total density n between 0.4 and 1.2. Similarly, in order to more efficiently collect statistics in nonzero polarization sectors, we tuned the chemical potentials in an anti-symmetric way with respect to the symmetric half-filling condition, i.e., $\mu_{1,2} = \mu_{\text{hf}} \pm \Delta\mu$, with μ_{hf} the chemical potential of the half filled symmetric binary mixture and $\Delta\mu$ chosen so as to access chains with polarizations m between -0.2 and 0.2 .

Acknowledgments: We thank T. Giamarchi for illuminating exchanges on incommensurate magnetism, D. Huse, A. Recati, E. Demler and F. Grusdt for helpful discussions and P. Sompet for critical reading of the manuscript. Financial support was provided by the Max Planck Society (MPG), the European Union (UQUAM, QSIMGAS, MIR-BOSE) and J.K. acknowledges funding from the Hector Fellow Academy.

Author Contributions: G. S., T. A. H., J. K., J. V.,

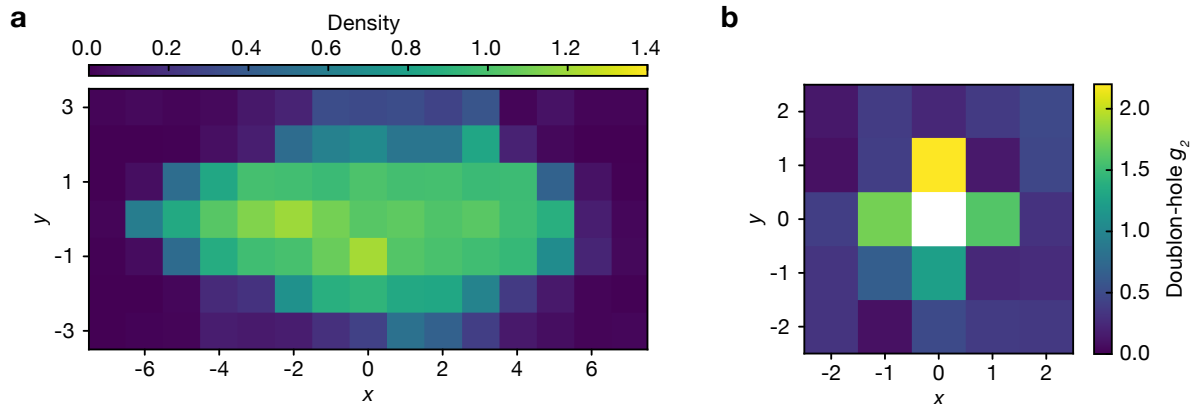


FIG. S4. **Properties of the prepared 2D clouds.** **a**, Density distribution for $t_y/t_x = 1$. **b**, Doublon-hole correlations $g_2(\vec{r})$. The strong bunching of the doubon-hole correlations $g_2(\vec{r})$ at $|\vec{r}| = 1$ justifies to discard outcomes where holes and doublons are found nearby when studying the effects of doping.

I. B. and C. G. planned the experiment, analyzed and discussed the data. J. N. and L. P. performed the QMC simulations. All authors contributed to the interpretation of the data and the writing.

Materials and Correspondence: Correspondence and requests for materials should be addressed to guillaume.salomon@mpq.mpg.de

* guillaume.salomon@mpq.mpg.de

- [1] T. Giamarchi, *Quantum Physics in One Dimension* (Clarendon Press, 2003).
- [2] D. Greif, T. Uehlinger, G. Jotzu, L. Tarruell, and T. Esslinger, *Science* **340**, 1307 (2013).
- [3] R. A. Hart, P. M. Duarte, T.-L. Yang, X. Liu, T. Paiva, E. Khatami, R. T. Scalettar, N. Trivedi, D. A. Huse, and R. G. Hulet, *Nature* **519**, 211 (2015).
- [4] M. F. Parsons, A. Mazurenko, C. S. Chiu, G. Ji, D. Greif, and M. Greiner, *Science* **353**, 1253 (2016).
- [5] M. Boll, T. A. Hilker, G. Salomon, A. Omran, J. Nespolo, L. Pollet, I. Bloch, and C. Gross, *Science* **353**, 1257 (2016).
- [6] L. W. Cheuk, M. A. Nichols, K. R. Lawrence, M. Okan, H. Zhang, E. Khatami, N. Trivedi, T. Paiva, M. Rigol, and M. W. Zwierlein, *Science* **353**, 1260 (2016).
- [7] J. H. Drewes, L. A. Miller, E. Cocchi, C. F. Chan, N. Wurz, M. Gall, D. Pertot, F. Brennecke, and M. Köhl, *Phys. Rev. Lett.* **118**, 170401 (2017).
- [8] P. T. Brown, D. Mitra, E. Guardado-Sanchez, P. Schauß, S. S. Kondov, E. Khatami, T. Paiva, N. Trivedi, D. A. Huse, and W. S. Bakr, *Science* **357**, 1385 (2017).
- [9] E. Dagotto, *Rev. Mod. Phys.* **66**, 763 (1994).
- [10] F. D. M. Haldane, *Journal of Physics C: Solid State Physics* **14**, 2585 (1981).
- [11] X. G. Wen, *Phys. Rev. B* **41**, 12838 (1990).
- [12] H. Frahm and V. E. Korepin, *Phys. Rev. B* **43**, 5653 (1991).
- [13] J. Cardy, *Scaling and Renormalization in Statistical Physics* (Cambridge University Press, 1996).
- [14] M. Bockrath, D. H. Cobden, J. Lu, A. G. Rinzler, R. E. Smalley, L. Balents, and P. L. McEuen, *Nature* **397**, 598 (1999).
- [15] J. Lee, S. Eggert, H. Kim, S.-J. Kahng, H. Shinohara, and Y. Kuk, *Phys. Rev. Lett.* **93**, 166403 (2004).
- [16] M. B. Stone, D. H. Reich, C. Broholm, K. Lefmann, C. Rischel, C. P. Landee, and M. M. Turnbull, *Phys. Rev. Lett.* **91**, 037205 (2003).
- [17] B. Lake, D. A. Tennant, C. D. Frost, and S. E. Nagler, *Nature Materials* **4**, 329 (2005).
- [18] M. Klanjšek, H. Mayaffre, C. Berthier, M. Horvatić, B. Chiari, O. Piovesana, P. Bouillot, C. Kollath, E. Orignac, R. Citro, and T. Giamarchi, *Phys. Rev. Lett.* **101**, 137207 (2008).
- [19] J. M. Tranquada, B. J. Sternlieb, J. D. Axe, Y. Nakamura, and S. Uchida, *Nature* **375**, 561 (1995).
- [20] A. Omran, M. Boll, T. A. Hilker, K. Kleinlein, G. Salomon, I. Bloch, and C. Gross, *Phys. Rev. Lett.* **115**, 263001 (2015).
- [21] T. A. Hilker, G. Salomon, F. Grusdt, A. Omran, M. Boll, E. Demler, I. Bloch, and C. Gross, *Science* **357**, 484 (2017).
- [22] H. V. Kruis, I. P. McCulloch, Z. Nussinov, and J. Zaanen, *Phys. Rev. B* **70**, 075109 (2004).
- [23] M. Ogata and H. Shiba, *Phys. Rev. B* **41**, 2326 (1990).
- [24] F. Woynarovich, *J. Phys. C Solid State* **15**, 85 (1982).
- [25] N. Bogoliubov, A. Izergin, and V. Korepin, *Nuclear Physics B* **275**, 687 (1986).
- [26] W. F. Brinkman and T. M. Rice, *Phys. Rev. B* **2**, 1324 (1970).
- [27] D. Greif, G. Jotzu, M. Messer, R. Desbuquois, and T. Esslinger, *Phys. Rev. Lett.* **115**, 260401 (2015).
- [28] S. R. White and I. Affleck, *Phys. Rev. B* **64**, 024411 (2001).
- [29] F. Grusdt, M. Kanasz-Nagy, A. Bohrdt, C. S. Chiu, G. Ji,

- M. Greiner, D. Greif, and E. Demler, arXiv:1712.01874 (2017).
- [30] E. Dagotto and T. M. Rice, *Science* **271**, 618 (1996).
- [31] S. R. White and D. J. Scalapino, *Phys. Rev. B* **55**, 6504 (1997).
- [32] S. R. White and D. J. Scalapino, *Phys. Rev. Lett.* **80**, 1272 (1998).
- [33] H. P. Büchler, *Phys. Rev. Lett.* **104**, 090402 (2010).
- [34] P. Jordan and E. Wigner, *Zeitschrift für Physik* **47**, 631 (1928).
- [35] N. V. Prokof'ev, B. V. Svistunov, and I. S. Tupitsyn, *Journal of Experimental and Theoretical Physics* **87**, 310 (1998).
- [36] L. Pollet, K. V. Houcke, and S. M. Rombouts, *Journal of Computational Physics* **225**, 2249 (2007).